

pubs.acs.org/JPCB Article

Which Physical Phenomena Determine the Ionization Potential of Liquid Water?

Jessica A. Martinez B,[△] Lukas Paetow,[△] Johannes Tölle, Xuecheng Shao,* Pablo Ramos, Johannes Neugebauer,* and Michele Pavanello*



Cite This: J. Phys. Chem. B 2023, 127, 5470-5480



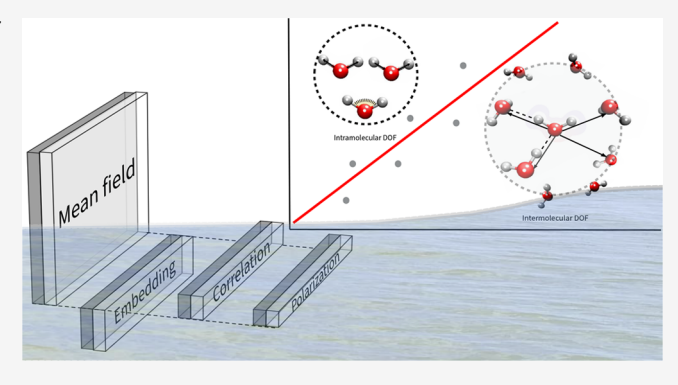
ACCESS I

Metrics & More

Article Recommendations

s Supporting Information

ABSTRACT: Understanding and predicting the properties of molecular liquids from the corresponding properties of the individual molecules is notoriously difficult because there is cooperative behavior among the molecules in the liquid. This is particularly relevant for water, where even the most fundamental molecular properties, such as the dipole moment, are radically different in the liquid compared to the gas phase. In this work, we focus on the ionization potential (IP) of liquid water by dissecting its individual contributions from the individual molecules making up the liquid. This is achieved by using periodic subsystem DFT, a state-of-the-art electronic structure method based on density embedding. We identify and evaluate four important electronic contributions to the IP of water: (1) mean-field, evaluated at the



Hartree—Fock level; (2) electronic correlation, incorporated via DFT and wave function-based methods; (3) interaction with and (4) polarization of the environment, both evaluated ab initio with density embedding. Furthermore, we analyze their impact on the IP relative to the structural fluctuation of liquid water, revealing unexpected, hidden correlations, confirming that the broadening of the photoelectron spectra is mostly caused by intermolecular interactions confined in the first solvation shell.

INTRODUCTION

Ionized states of molecules and materials take part in many crucial processes in electrochemistry and photochemistry, as well as peculiar states of matter like excess electrons solvated in liquids. The high-accuracy determination of the ionization potential (IP) of condensed-phase molecular systems such as liquid water have represented a major challenge in recent years in both experimental and computational fields. However, recent advances in liquid microjet (LJ) photoelectron spectroscopy have opened the door to the determination of accurate electronic energetics of water and aqueous solutions.^{2–5} From a computational perspective, there is a long history regarding the IP of liquid water.^{6,7} Recently, Gaiduk et al.⁸ have employed models given by Born-Oppenheimer (BO) and path-integral (PI) molecular dynamics simulations carried out with a polarizable many-body potential (MB-pol)⁹ and simulated the IPs using many-body perturbation theory with the G_0W_0 approximation. To inspect the effect of self-consistency in the GW approach, Ziaei et al.¹⁰ employed a self-consistent GW approach with vertex correction, 11 finding good agreement with the averaged IP results of Gaiduk et al.8 The Herbert group employed resolution of the identity MP2, including a shell of explicit water molecules with long-ranged Coulomb interactions handled by Poisson boundary conditions and obtained average

IP values in good agreement with the experiments and the listed simulations. ¹²

The aim of this work is not to simply provide an average IP value for water, but rather to understand the entire photoelectron spectral line, including its broadening, from the viewpoint of the single water molecules making up the bulk. Understanding the fundamental physical and chemical properties of molecular condensed phase systems by their elementary building blocks (individual molecules) has been of great interest for decades.¹³ Intuitively, such an approach is feasible provided that the interactions between the molecules in the condensed phase are weak. Unfortunately, intermolecular interactions in condensed phases can range from very weak to very strong, with a significant gray area in between where, unfortunately, liquid water is located. For example, for this fundamental liquid, it was estimated that the molecular dipole in the liquid is 2.6 D compared to the dipole in the gas phase of only 1.8 D. 14 There are other examples, e.g., the first electronic excitation energy

Received: October 31, 2022 Revised: May 4, 2023 Published: June 2, 2023





band of water is much broader for the liquid phase compared to the gas phase. This is such that the onset of the band of the liquid phase is red-shifted compared to the gas phase, while the maximum is blue-shifted. Yet, the broadening of the excitation band was shown to be entirely due to the intermolecular interactions occurring within the first solvation shell. Therefore, the difficulty (or impossibility) to predict the properties of water from the properties of the isolated water molecules is clear and likely applicable to the IP.

In fact, there is a large body of work on the analysis of photoelectron spectra in terms of the local hydrogen bond network surrounding a given water molecule in the liquid. The main conclusion of the mentioned works is that the immediate surrounding of a water molecule and, specifically, the number of donated hydrogen bonds (which dynamically fluctuates 20) are responsible for the broadening of the $1b_1$ peak in the liquid phase compared to the gas phase. In all cases, the broadening of the photoelectron spectral lines could only be qualitatively discussed.

To attack this issue, to shed light on the root causes of the broadening of the photoelectron spectrum of liquid water, in this work, for the first time, we dissect its IP into four major contributions, which we identify as follows: (1) Mean-field: the vertical ionization potential of each water molecule composing the bulk computed at the mean-field, Hartree–Fock level; (2) Correlation: the effect of going beyond Hartree-Fock to account for electronic correlation within each water molecule at the correlated wave function level as well as with DFT methods; (3) Embedding: comprises the Coulomb interactions between each (ionizing) water molecule and their environment, defined as an infinite bulk of water augmented by effects of exchange, correlation, and Pauli repulsion (nonadditive kinetic energy); and (4) Polarization: This contribution is identified with the energy shift of the interaction energy among neutral molecules constituting the environment of an ionizing molecule compared with a neutral molecule.

For each of the four contributions to the IP, we carry out a meticulous analysis of its dependence on the molecular-level structure of the liquid. By using subsystem DFT (sDFT)²¹ to determine the electronic structure of the system, we are able to analyze the ionization of each water molecule making up the liquid on an equal footing and individually. In turn, we can probe the entirety of the photoelectron spectrum band for the first ionization of water, the so-called $1b_1$ peak.

To achieve such a granular description of the ionization process, we choose the Δ SCF procedure, which prescribes the computation of the total energies of the ionized and neutral states, and their difference identifies the IP. This may cause worry, as no off-the-shelf electronic structure software can apply periodic boundary conditions for modeling bulk systems having a non-neutral total charge with corrected (nondivergent) energies and potentials. In a previous work by some of us, ²² we presented a new sDFT method capable of approaching charged systems, regardless of the underlying adoption of periodic boundary conditions.

THEORETICAL BACKGROUND

In this work, we exploit the ability of sDFT to express the electronic structure of a system as a sum of subsystem contributions. This will also allow us to express the IP of water as a collection of ionizations for each water molecule in the bulk. By computing the IP contribution arising from each water

molecule, we are able to correlate it to the molecular structure and its environment.

The total Kohn–Sham (KS) DFT energy of an electronic system is exclusively a functional of the electron density, $\rho(\mathbf{r})$, and reads as,

$$E[\rho] = T_{s}[\rho] + V_{nuc}[\rho] + E_{H}[\rho] + E_{xc}[\rho]$$
 (1)

where $V_{\rm nuc}[\rho] = \int \rho({\bf r}) v_{\rm ext}({\bf r}) d{\bf r}$, and $E_{\rm H}[\rho]$, and $E_{\rm xc}[\rho]$ are the Hartree and exchange-correlation energy functionals, and $T_{\rm s}[\rho]$ accounts for the total kinetic energy of the system.

The above leads to the definition of the KS equation,

$$\left(-\frac{\nabla_{i}^{2}}{2} + \nu_{\text{ext}}(\mathbf{r}) + \nu_{\text{H}}[\rho](\mathbf{r}) + \nu_{\text{xc}}[\rho](\mathbf{r})\right) \psi_{i}(\mathbf{r}) = \varepsilon_{i} \psi_{i}(\mathbf{r})$$
(2)

In which, $v_{\rm ext}({\bf r})$ denotes the external potential, and $v_{\rm H}[\rho]({\bf r})$ and $v_{\rm xc}[\rho]({\bf r})$ represent the electronic Coulomb (Hartree) and the exchange-correlation potentials.

Subsystem DFT (sDFT). sDFT employs a divide-and-conquer approach, where the total system (a model of bulk water in this work) is split into interacting fragments, called subsystems. The subsystems are small in size compared to the total system. ²¹ The electron density of the total system is partitioned into subsystem electron densities, $\{\rho_I(\mathbf{r})\}$, and written as

$$\rho(\mathbf{r}) = \sum_{I=1}^{N_{\rm S}} \rho_I(\mathbf{r}) \tag{3}$$

where N_S is the total number of subsystems.

The total electronic energy in sDFT is defined as a functional of all the subsystem densities. Namely,

$$E[\{\rho_I\}] = \sum_I T_{\rm s}[\rho_I] + V_{\rm nuc}[\rho] + E_{\rm H}[\rho] + E_{\rm xc}[\rho] + T_{\rm s}^{\rm nad}[\{\rho_I\}] \tag{4} \label{eq:energy}$$

where $V_{\text{nuc}}[\rho] = \int \rho(\mathbf{r}) v_{\text{ext}}(\mathbf{r}) d\mathbf{r}$, and $E_{\text{H}}[\rho]$ and $E_{\text{xc}}[\rho]$ are the Hartree and exchange-correlation energy functionals.

The electronic energy just presented in sDFT can also be expressed as the sum of additive and nonadditive energy terms,

$$E[\{\rho_{I}\}] = \sum_{I} E_{I}[\rho_{I}] + E^{\text{nad}}[\{\rho_{I}\}]$$
(5)

The additive part is calculated using the ground state Kohn–Sham-DFT functional computed with the external potential of subsystem I, $v_{\rm ext}^I({\bf r})$. We remark that the total external potential in eq 4 is given by the sum of all subsystem external potentials, $v_{\rm ext}({\bf r}) = \sum_I^{N_{\rm S}} v_{\rm ext}^I({\bf r})$. The nonadditive energy is given by three terms (equations below): Coulomb $E_{\rm Coul}^{\rm nad}[\{\rho_I\}]$ in eq 6, exchange-correlation $E_{\rm xc}^{\rm nad}[\{\rho_I\}]$ in eq 7, and the nonadditive kinetic energy $T_{\rm sc}^{\rm nad}[\{\rho_I\}]$ in eq 8. They are defined as follows,

$$E_{\text{Coul}}^{\text{nad}}[\{\rho_I\}] = \sum_{I,J \neq I}^{N_s} \int \rho_I(r) v_{\text{ext}}^J(\mathbf{r}) dr + \left(E_{\text{H}}[\rho] - \sum_{I=1}^{N_s} E_{\text{H}}[\rho_I] \right)$$
(6)

$$E_{\rm xc}^{\rm nad}[\{\rho_I\}] = E_{\rm xc}[\rho] - \sum_{I=1}^{N_{\rm S}} E_{\rm xc}[\rho_I]$$
 (7)

$$T_{s}^{\text{nad}}[\{\rho_{I}\}] = T_{s}[\rho] - \sum_{I=1}^{N_{s}} T_{s}[\rho_{I}]$$
 (8)

The additive part of the kinetic energy is evaluated exactly from the subsystem KS orbitals,

 $T_{\rm s}[\rho_I] \equiv T_{\rm s}[\{\psi_i^I({\bf r})\}] \equiv \sum_i \left\langle \psi_i^I \middle| -\frac{1}{2} \nabla^2 \middle| \psi_i^I \right\rangle$. Generally, in practical calculations, the nonadditive kinetic energy $T_{\rm s}^{\rm nad}[\{\rho_I\}]$ is evaluated approximately with pure density functionals, such as revAPBEK.²³

The variational problem in sDFT is given by the set of KS equations with constrained electron density,²⁴ which read

$$\left(-\frac{\nabla_{i}^{2}}{2} + v_{\text{eff}}^{I}[\rho_{I}](\mathbf{r}) + v_{\text{emb}}^{I}[\rho_{I}, \rho](\mathbf{r})\right) \psi_{i}^{I}(\mathbf{r}) = \varepsilon_{i}^{I} \psi_{i}^{I}(\mathbf{r})$$
(9)

where the subsystem-specific effective KS potential contains the intrasubsystem contributions and is defined as

$$v_{\text{eff}}^{I}[\rho_{I}](\mathbf{r}) = v_{\text{ext}}^{I}(\mathbf{r}) + v_{\text{H}}[\rho_{I}](\mathbf{r}) + v_{\text{xc}}[\rho_{I}](\mathbf{r})$$
(10)

In the above equation, $v_H[\rho_I](\mathbf{r})$ and $v_{xc}[\rho_I](\mathbf{r})$ represent the electronic Coulomb and the exchange-correlation potentials arising from the electron density of subsystem I. The interaction of the electrons of subsystem I with the environment is represented by an embedding potential that reads as follows,

$$v_{\text{emb}}^{I}[\rho_{I}, \rho](\mathbf{r}) = \sum_{J,J \neq I} \left[v_{\text{ext}}^{J}(\mathbf{r}) + v_{\text{H}}[\rho_{J}](\mathbf{r})\right] + v_{\text{xc}}^{\text{nad}}[\{\rho_{I}\}](\mathbf{r}) + v_{T_{s}}^{\text{nad}}[\{\rho_{I}\}](\mathbf{r})$$

$$(11)$$

The nonadditive exchange-correlation potential $v_{\rm xc}^{\rm nad}[\{\rho_I\}]({\bf r})$ and the nonadditive kinetic potential $v_{\rm xc}^{\rm nad}[\{\rho_I\}]({\bf r})$ are defined as in eq 12 and eq 13,

$$\nu_{\rm xc}^{\rm nad}[\{\rho_I\}](\mathbf{r}) = \frac{\delta E_{\rm xc}[\rho]}{\delta \rho(\mathbf{r})} - \frac{\delta E_{\rm xc}[\rho_I]}{\delta \rho_I(\mathbf{r})}$$
(12)

$$v_{T_s}^{\text{nad}}[\{\rho_I\}](\mathbf{r}) = \frac{\delta T_s[\rho]}{\delta \rho(\mathbf{r})} - \frac{\delta T_s[\rho_I]}{\delta \rho_I(\mathbf{r})}$$
(13)

The subsystem orbital energies are denoted by ε_i^I in eq 9.²¹ We remark that, in practice, the set of subsystem KS equations can either be solved iteratively using a Freeze-and-Thaw²⁵ procedure, or simultaneously for all subsystems with the total density being updated at every SCF cycle.^{26–29}

Calculating the Ionization Potential. To compute the IP, we use a Δ SCF procedure by taking the difference between the total energy of the neutral system, E_{tot}^0 and the total energy of the charged system (one electron removed), E_{tot}^+

$$IP = E_{\text{tot}}^+ - E_{\text{tot}}^0 \tag{14}$$

To describe the bulk, we employ periodic boundary conditions (PBC) with simulation cells containing a limited number of molecules (64 in this work). The IP of liquid water is therefore sampled over the 64 water molecules in the simulation cell. This is repeated for several snapshot configurations (vide infra).

We thus have an opportunity and a potential problem. On one side, we can use sDFT to compute the electronic structure of ionized systems. This avoids charge-density overdelocalization issues originating from possible self-interaction error in the exchange-correlation density functional. Additionally, sDFT's computational complexity is advantageous, as it scales quasi-linearly with the number of subsystems involved. Con the other side, because of the need to employ PBC to approach bulk systems, the total energy of charged systems is not directly accessible. The next section outlines a workaround for this problem which we call "impurity model".

Putting the issue of charged systems in periodic boundary conditions aside for the moment, the advantages of using sDFT for computing the IP of bulk molecular liquids are enormous. First and foremost, the subsystem electronic structure can be computed with any electronic structure method one desires. Typically the molecules in a molecular liquid are small and almost any quantum chemistry method can be applied (perhaps with exception of full CI). Thus, an accurate description of the intrasubsystem electronic structure is at hand (vide infra, in this work we will use semilocal DFT as well as MP2 and coupled cluster methods). Additionally, because sDFT dissects the total energy into additive and nonadditive terms we have the opportunity to further break down the IP in such a granular way that is inaccessible by standard electronic structure methods.

To compute eq 14 we express the energies of cation and neutral species according to eq 5. Hereafter, we will indicate the ionized subsystem with the notation ρ_I^+ , while when we use a different index counter, e.g., ρ_J^+ , we imply that subsystem J is a neutral subsystem polarized by the ionized subsystem I. For clarity, the expression of the cation/neutral energies is summarized as,

$$E_{\text{tot}}^{+} \equiv E[\{\rho_{J}^{+}\}, \rho_{I}^{+}] = \sum_{J}^{N_{c}} E_{J}[\rho_{J}^{+}] + E^{\text{nad}}[\{\rho_{J}^{+}\}, \rho_{I}^{+}]$$
(15)

$$E_{\text{tot}}^{0} \equiv E[\{\rho_{J}^{0}\}] = \sum_{J}^{N_{s}} E_{J}[\rho_{J}^{0}] + E^{\text{nad}}[\{\rho_{J}^{0}\}]$$
(16)

where we have introduced a notation of the electron density with a +/0 The nomenclature is summarized in eq 17.

 $\rho_{\rm I}^+ \ \ \, \rightarrow \, {\rm density} \, {\rm of} \, {\rm ionized} \, {\rm subsystem} \, \, I,$

 $o_i^+ \rightarrow \text{density of neutral subsystem } J \text{ polarized by ionized subsystem } I$,

$$ho_{I/J}^0
ightarrow {
m density}$$
 of neutral subsystems I/J part of the neutral system (17)

In this work we partition the IP in the following manner:

(1) Mean-field: the Hartree—Fock energy difference between an ionized and the corresponding neutral water molecule subsystem, where the electronic structure of the molecule is computed in the field provided by the environment subsystems. Using the previously introduced nomenclature in eq 17,

$$IP_{\rm HF} = E_I^{\rm HF}[\rho_I^{+,{\rm HF}}] - E_I^{\rm HF}[\rho_I^{0,{\rm HF}}]$$
 (18)

In the above equation, $E_I^{\rm HF}$ is the HF energy functional of the isolated subsystem I evaluated with the density (or, more precisely, the corresponding set of orbitals) given in the argument, and $\rho_I^{+/0,{\rm HF}}$ represents the corresponding densities computed self-consistently with the HF Fock operator augmented by a static embedding potential derived from a separate sDFT calculation that was carried out at the PBE level in periodic boundary conditions. It is important to note that the energies used in eq 18 do not include the interaction with the environment, i.e., they are the "internal" energies of the water molecule in the two electronic states considered (neutral and charged).

(2) Electronic Correlation: the difference between an IP calculated with eq 18 and an IP calculated with the same equation with the HF functional replaced by a method

that accounts for electronic correlation (e.g., Coupled cluster, MP2, and DFT).

(3) Embedding or Interaction: comprised of two parts. The first one is the Coulomb interaction between the ionized water molecule (subsystem) and the environment. We define this contribution by considering the following integral of the density of the ionized molecule $[\rho^{+/0}(\mathbf{r})]$ for the ionized/neutral molecule with their corresponding embedding potentials $[\nu_{\rm emb}^{+/0}(\mathbf{r})]$ stripped of the non-additive $T_{\rm s}$ and xc contributions. Namely,

$$\Delta IP_{\text{emb}} = \sum_{I}^{N_s} \int \tilde{v}_{\text{emb}}^{I,+}(\mathbf{r}) \rho_I^{+}(\mathbf{r}) d\mathbf{r} - \sum_{I}^{N_s} \int \tilde{v}_{\text{emb}}^{I,0}(\mathbf{r}) \rho_I^{0}(\mathbf{r}) d\mathbf{r}$$
(19)

where

$$\tilde{\nu}_{emb}^{I,+/0}({\bf r}) = \nu_{emb}^{I,+/0}({\bf r}) \, - \, \nu_{T_s}^{nad,I,+/0}({\bf r}) \, - \, \nu_{xc}^{nad,I,+/0}({\bf r}).$$

The second part of the embedding contribution accounts for the nonadditive exchange-correlation and kinetic energy (T_s) , which are evaluated directly using eqs 7 and 8. Therefore, the complete expression of the embedding contribution is given by,

$$\Delta IP_{emb} = \sum_{I}^{N_{s}} \int \tilde{v}_{emb}^{I,+}(\mathbf{r}) \rho_{I}^{+}(\mathbf{r}) - \sum_{I}^{N_{s}} \int \tilde{v}_{emb}^{I,0}(\mathbf{r}) \rho_{I}^{0}(\mathbf{r})$$

$$+ \left(E_{xc}[\rho^{+}] - \sum_{J \neq I}^{N_{S}} E_{xc}[\rho_{J}^{+}] - E_{xc}[\rho_{I}^{+}] - E_{xc}[\rho^{0}] \right)$$

$$+ \sum_{J=1}^{N_{S}} E_{xc}[\rho_{J}^{0}] + \left(T_{s}[\rho^{+}] - \sum_{J \neq I}^{N_{S}} T_{s}[\rho_{J}^{+}] - T_{s}[\rho_{I}^{+}] \right)$$

$$- T_{s}[\rho^{0}] + \sum_{J=1}^{N_{S}} T_{s}[\rho_{J}^{0}]$$
(20)

(4) Polarization: This contribution to the IP arises from the energy associated with the polarization of the environment due to the presence of a charged subsystem compared to a neutral subsystem captured by computing two terms, ΔIP_{pol}⁽¹⁾ and ΔIP_{pol}⁽²⁾. ΔIP_{pol}⁽¹⁾ measures the change in the strength of the interaction between the water molecules in the environment. ΔIP_{pol}⁽²⁾ accounts for the change in the internal energy of the water molecules in the environment. The definitions of the two terms are found in eqs 21 and 22.

$$\Delta IP_{\text{pol}}^{(1)} = \left(E_{\text{Coul}} \left[\sum_{j \neq I}^{N_s} \rho_j^+ \right] - \sum_{j \neq I}^{N_s} E_{\text{Coul}}[\rho_j^+] \right)$$

$$- \left(E_{\text{Coul}} \left[\sum_{j \neq I}^{N_s} \rho_j^0 \right] - \sum_{j \neq I}^{N_s} E_{\text{Coul}}[\rho_j^0] \right)$$

$$(21)$$

$$\Delta IP_{\text{pol}}^{(2)} = \sum_{J \neq I}^{N_s} (E_J[\rho_J^+] - E_J[\rho_J^0])$$
(22)

In conclusion, by summing up the reported four contributions, the final value of the IP is obtained for each water molecule considered in the model. The final reported value of the IP is simply the average of the IP of each water molecule in each geometry snapshot considered. We also histogram the IPs of all water molecules in all snapshots to compare directly with the experimental photoelectron spectrum. 5,38

The Impurity Model. The impurity model is based on the simple realization that a subsystem electron density can be considered either as the density of an extended, periodically repeating subsystem or the density of a finite, single subsystem. In practical calculations the finite and the extended subsystems are defined by the way the Coulomb potentials for the electronic and nuclear charges are computed in the intra- and intersubsystem potential.

When a finite subsystem is considered, the electronic Coulomb embedding potential is augmented by a screening potential to become

$$\nu_{H}^{\text{emb},I}[\{\rho_{J}\}](\mathbf{r}) = \nu_{H} \left[\sum_{J \neq I} \rho_{J} \right] (\mathbf{r}) + \nu_{H}^{\text{screen}}[\rho_{I}](\mathbf{r})$$
(23)

where formally $v_H[\sum_{J\neq I}\rho_J](\mathbf{r}) = v_H[\rho - \rho_I](\mathbf{r})$ is the periodic electronic Coulomb potential of the environment density $\rho - \rho_I$ and the screening potential reads

$$v_{\rm H}^{\rm screen}[\rho_I](\mathbf{r}) = v_{\rm H}[\rho_I](\mathbf{r}) - \overline{v}_{\rm H}[\rho_I](\mathbf{r})$$
(24)

where $\overline{\nu}_{\rm H}$ is the electronic Coulomb potential of a finite, nonperiodic subsystem with density $\rho_{\rm I}$. The screening potential essentially is the contribution of the embedding potential from the periodic images of the same subsystem. Therefore, the impurity model achieves the goal of generating a partition of the system into one finite, nonperiodic subsystem with density $\rho_{\rm I}$ and a semi-infinite environment. Such an impurity model is then applied to the nuclear Coulomb potential as well.

The screening potential for a charged subsystem is somewhat more involved because one wishes to only keep the charged subsystem in one lattice site and in all other periodic images one replaces the charged subsystem with a neutral subsystem. This can be achieved by considering the following screening potential which must depend on the subsystem electron densities of the neutral and charged versions, $\rho_I^{0,+}$, of subsystem *I*. Namely,

$$v_{\rm H}^{\rm screen}[\rho_{\rm r}^0, \rho_{\rm r}^+](\mathbf{r}) = v_{\rm H}^{\rm screen}[\rho_{\rm r}^0](\mathbf{r}) - v_{\rm H}^{\rm screen}[\rho_{\rm r}^+](\mathbf{r}) + \Delta_0[\rho_{\rm r}^0, \rho_{\rm r}^+] \tag{25}$$

where Δ_0 is a constant shift added to the embedding potential to reference consistently neutral and charged systems (i.e., the so-called G=0 correction, see ref 37) and $v_{\rm H}^{\rm screen}[\rho_I^+]$ is computed with eq 24 with the neutral subsystem density replaced by the charged subsystem density. The G=0 correction can be computed in several ways, for example it can be evaluated assuming that a slab's potential reaches the vacuum level, ³⁹⁸ from analytical considerations, ⁴⁰ or with numerical Fourier transforms. ³⁷ In the impurity model, we employ the latter. We stress that the impurity model carries an important advantage compared to several other methods that deal with the divergences of the Coulomb terms of charged systems in PBC, ⁴⁰ in that it corrects both the energy and the electrostatic potential. Therefore, in principle, it delivers subsystem electron densities that are (self)consistent with respect to the energy functional used and the boundary conditions employed. ²²

We introduce a minor approximation in the implementation of the impurity model, i.e., in our definition of the auxiliary neutral subsystem density in eq 25, ρ_I^0 . This is typically borrowed from a separate calculation of a neutral system. In our previous work, we assessed the effect of including a self-consistently determined ρ_I^0 to find a very small correction to the energy. Thus, in this work we will only consider non-self-consistent ρ_I^0 for the determination of the embedding potentials within the impurity model of eq 25.

RESULTS

A summary of the various contributions to the average vertical IP of bulk liquid water is presented in Figure 1 for both the PI and

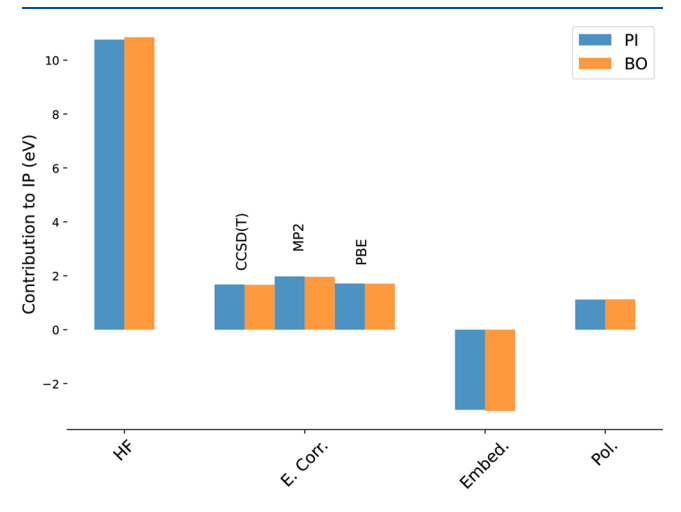


Figure 1. IP of bulk liquid water broken down into four major contributions: Mean-field Hartree–Fock (HF), electronic correlation (E. Corr.), the interaction with the environment (Embed.), and the polarization of the environment (Pol.).

the BO AIMD snapshots. Hereafter, we will simply refer to the computed vertical IP as IP. The mean-field Hartree-Fock contribution averages to 10.85 (10.76) eV for the BO (PI) snapshots. The electron correlation contribution increases the mean-field HF IP by 16% or 1.67 (1.68) eV at the CCSD(T) level. In the figure we also feature the correlation energy contribution from other methods, such as DFT (PBE XC functional) and MP2. As expected, 41,42 MP2 overestimates the correlation energy by about 0.30 eV compared to CCSD(T). The polarization contribution also is significant, averaging to 1.13 (1.12) eV. However, the biggest contribution, second only to the mean-field IP, is the embedding contribution arising from the interaction of the ionizing molecule with the environment. This accounts for a reduction of the IP by close to 3 eV. The IP reduction from the embedding contribution makes physical sense as the cation is more strongly stabilized by the interaction with the polar environment than the neutral molecule.

It is clear that there is a curious interplay between the various contributions to the IP. Some are positive (increasing the IP) others are negative (decreasing the IP). It is interesting to inspect whether these contributions have different intrinsic dependencies on the structural degrees of freedom of the liquid. For example, some may only depend on degrees of freedom internal to the single ionizing water molecule. Others may display a dependency on intermolecular degrees of freedom. We present such an analysis later.

A question may arise regarding the role of the potential delocalization of the positive charge (hole) to water molecules surrounding the cation. To shed light on this possibility, we have computed the electronic couplings with the transfer integrals method (see refs 43 and 44 for details) between states where the hole is localized on one molecule or another for all molecule pairs in the system cut off by a radius of 6 Å. We found that, upon diagonalization of the ensuing Hamiltonian (which has the CCSD(T) IPs on the diagonals and the computed couplings on the off-diagonals), the average IP increased by merely 0.005 eV. Thus, we conclude that delocalization of the hole among more

than one molecule does not significantly influence the IP of liquid water.

In ref 45, Ambrosio and Pasquarello showed that when employing a carefully calibrated exchange-correlation functional approximation (PBEh(40)-rVV10), the wave function of a hole in liquid water following a vertial ionization, rather than being localized on a single water molecule, it is delocalized over several water molecules. The reader might confuse our model involving sequential ionizations of single water molecules as a major approximation. However, we lift this approximation by computing hole transfer coupling between the localized, "diabatic" states (see computational details). The resulting Hamiltonian and overlap matrices are then diagonalized giving proper "adiabatic" states that might display a certain level of hole delocalization that we have not analyzed. Independent from this, our results show that the resulting IP histogram of the adiabatic IP values follows closely the one of the diabatic IP values. Therefore, we continue our analysis using the diabatic IP values simply as a matter of computational convenience.

IP Contributions and Their Correlation with Intra- and Intermolecular Degrees of Freedom. Mean-Field HF and Electronic Correlation Contribution. The correlation coefficients between the structural (intra- and intermolecular) degrees of freedom and the individual IP contributions were calculated for both the PI and the BO MD snapshots. The symmetric (Sym. vib.) and antisymmetric (Antisym. vib.) O—H stretch vibrations of a given water molecule as well as the HOH angle constitute the intramolecular degrees of freedom that were investigated. Recent investigations of the photoemission spectrum of water point to the important role of hydrogen bonds for the explanation of certain features of the spectrum. Therefore, in this section we include donated and accepted hydrogen bonds (H-bonds) as intermolecular order parameters that we will correlate with the value of the IP.

We also consider a composite order parameter aimed at measuring the size of the first solvation shell (d1-d4). The d1-d4 order parameter is a linear combination of the four closest oxygen—oxygen distances (d1, d2, d3, d4). Specifically, d4 = $\sum_i c_i di$. The expansion coefficients, $\{c_i\}$, are determined by a linear regression against the IP values (we remark that regressions other than linear have been considered and yield very similar results). See Figure 2 for a depiction of the degrees of freedom considered.

The correlation coefficients for mean-field HF and the electronic correlation contribution are shown in Figure 3. HF correlates the most with Sym. vib. (-0.94 and -0.88 for the PI) and BO snapshots, respectively). The correlation coefficients of HF with the other degrees of freedom remain below 0.33 in magnitude.

We notice that the electronic correlation contribution has highest correlation coefficient with the Sym. vib. (0.69 and 0.41 for PI and BO snapshots, respectively), while the correlation coefficients with the other degrees of freedom do not exceed 0.30 in magnitude. This is a result that compares well with past studies carried out in the gas phase. We note that generally we see higher correlations for the PI snapshots. This is likely because PI MD allows the water molecules to probe a larger region of phase space compared to BO MD due to the additional forces originating from the path integral ring polymers. 47

Embedding and Polarization Contributions. In Figure 4, we show the correlation coefficients of the embedding and polarization contributions to the IP. Inspecting the figure, it is clear that with a correlation of below 0.1, embedding does not

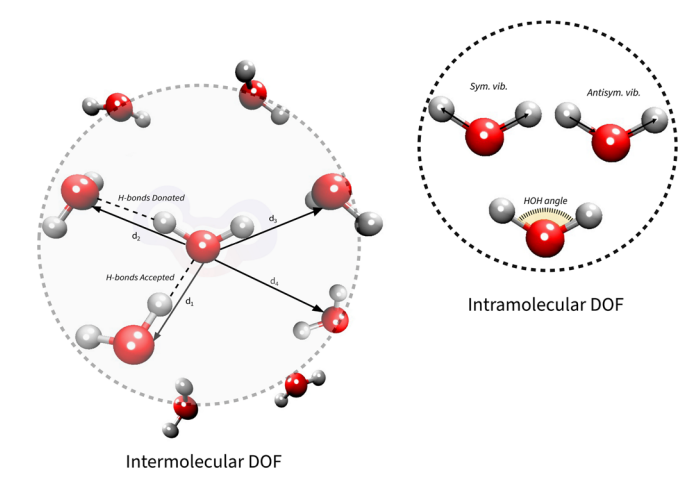


Figure 2. Schematic representation of intra- and intermolecular degrees of freedom. Intermolecular: H-bonds donated, H-bonds accepted by the ionizing water molecule, and oxygen—oxygen distance from the central (ionized) water molecule to the four nearest neighbors. Intramolecular: Symmetric OH stretch vibration (Sym. vib.), Antisymmetric OH stretch vibration (Antisym. vib.), and HOH angle.

correlate well with d1-d4. On the other hand, polarization shows a weak anticorrelation of -0.35. Therefore, it is not surprising to note that for the sum of embedding and polarization (right-most panel in Figure 4) the correlation with respect to d1-d4 remains below 0.15 (a negligible value).

We have determined that this behavior is not particular to d1-d4, but that it applies to most correlation coefficients with the oxygen—oxygen distances up to the 10-th closest molecule to the ionizing molecule, see Figures 5 and S4 in the Supporting Information. A similar correlation with the position of nearby water molecules was noticed in previous studies 7,19 as well as in an analysis by some of the authors concerning the low-lying excitation energies of water. 18

A similar behavior is observed for the amount of H-bonds donated, where the embedding and polarization contributions display correlation coefficients that are of the opposite sign, respectively. Regarding the number of H-bonds accepted, we found an almost negligible correlation from the polarization contribution, while embedding shows weak but nonnegligible correlation coefficients (-0.29 and -0.32).

Finally, we briefly discuss a comparison between the IP of the liquid compared to the one of the vapor. We obtain the IP of the

vapor by borrowing the geometries of each water molecule from the PI or BO snaphots, but then we treat each molecule as an isolated system. This should give us a measure of the embedding effect given by the condensed phase. Tables S1 and S2 and Figure S5 in the Supporting Information show that the gas phase IP is much higher than the liquid IP (by about 2 eV). This is reminiscent of a similar shift in the optical spectrum of liquid water. ^{18,48–50}

Account of Nuclear Quantum Effects and Comparison With Experimental IPs. Gaiduk et al.⁸ estimated that the inclusion of nuclear quantum effects (NQE) has a small effect on the average IP (less than 0.1 eV). However, they showed that the distribution of the dipole moments of the water molecules in the liquid is broader when calculated from the PI snapshots compared to BO. Thus, we expect that including nuclear quantum effects will result in a broadening of the IP distribution and a small shift of the average IP. In Figure 6, we report our results for the IP distribution at the CCSD(T) level (the IP values include the sum of all contributions). Inspecting the figure, we confirm that the PI MD snapshots result in a broader IP distribution. We also inspect the linear extrapolation of the IP to find the value of the valence band maximum (VBM, see Table S2). Chen et al.⁵¹ predict a strong renormalization of 0.2 eV for the VBM when NQE are taken into account. In order to compare our results with refs 51 and 52 we report the values of the extrapolation to low IP values of our IP histograms (equivalent to the extrapolated VBM) for our simulations as well as the ones of Gaiduk et al. in Table S2 of the Supporting Information. Our VBM shift due to NQEs is 0.33 eV for PBE, 0.31 eV for CCSD(T) and 0.25 eV for MP2. Gaiduk et al. find it to be 0.32 and 0.29 eV when GW/PBE or GW/RSH are used, respectively.

From the values reported in Table 1, we can also see that the average IPs do not shift considerably upon accounting for NQE, regardless of the methods employed.

When comparing our results with the literature, we note that our values underestimate the measured IP of bulk liquid water by about 0.70-0.75 eV when we employ CCSD(T) and 0.53-0.57 eV when we employ MP2.

The discrepancy is due to approximations in our simulations. The most consequential approximation is the finite-size effect related to the polarization of the water molecules in the environment. This is in line with previous works based on cluster models and continuum boundary conditions. ^{55–57} In Table S4

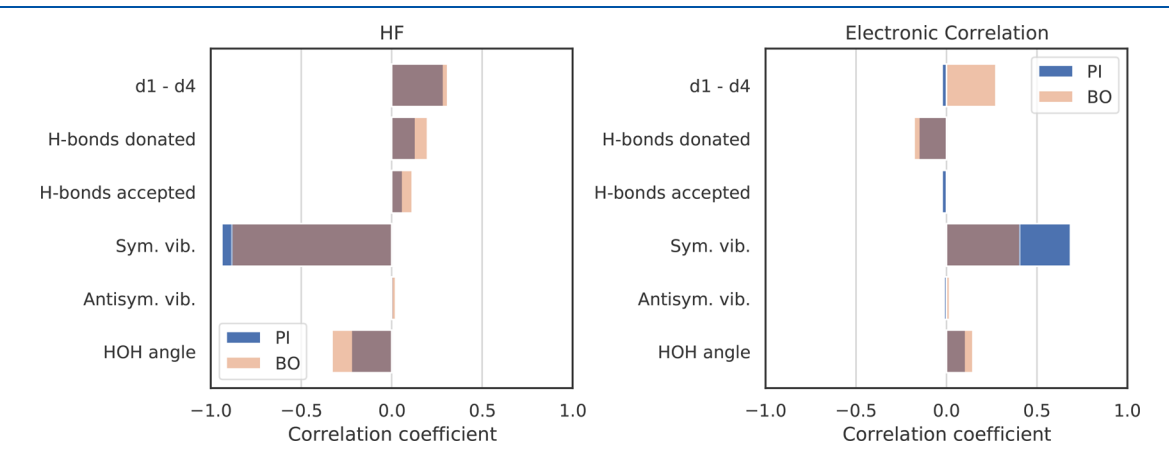


Figure 3. Correlation coefficients for the HF and the electronic correlation (reported here computed with CCSD(T)) contributions to the IP of liquid water with the selected structural degrees of freedom for the PI and BO snaphots.

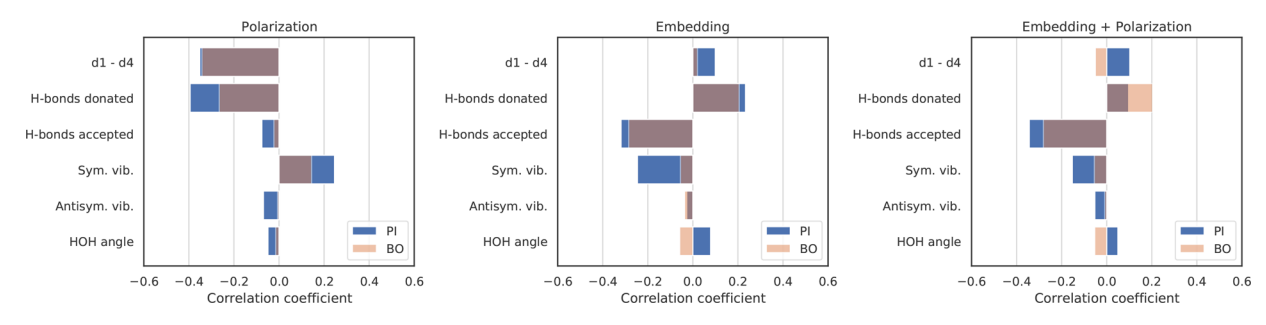


Figure 4. Correlation coefficients between the molecular degrees of freedom and the embedding and polarization contributions to the IP of water for both the PI and BO MD snapshots.

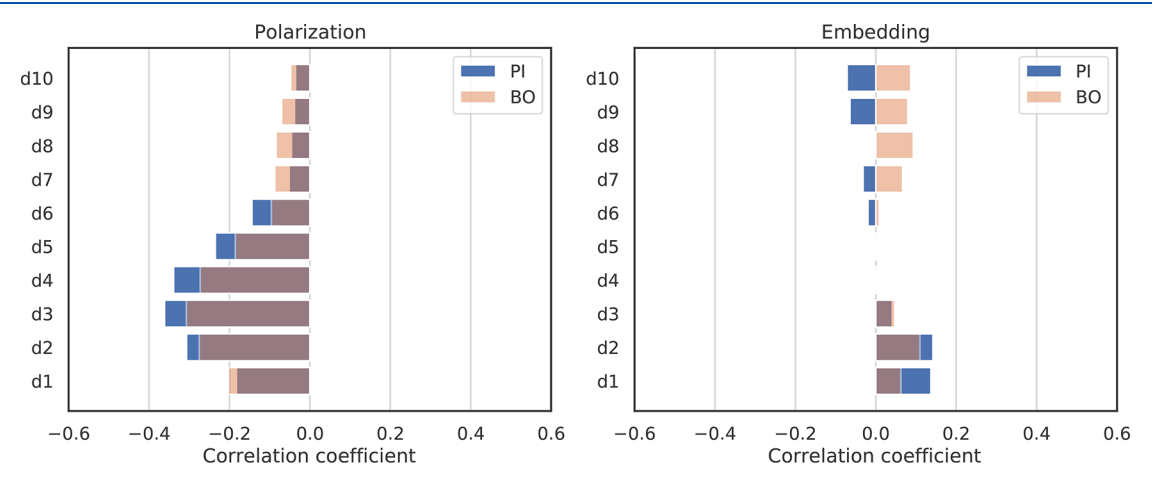


Figure 5. Correlation coefficients between electronic correlation energy (CCSD(T)) of liquid water with the respective average distance to the n'th neighboring water molecule (dn). These data were taken from 10 snapshots of the 64 water molecule systems from PI and BO MD trajectories.

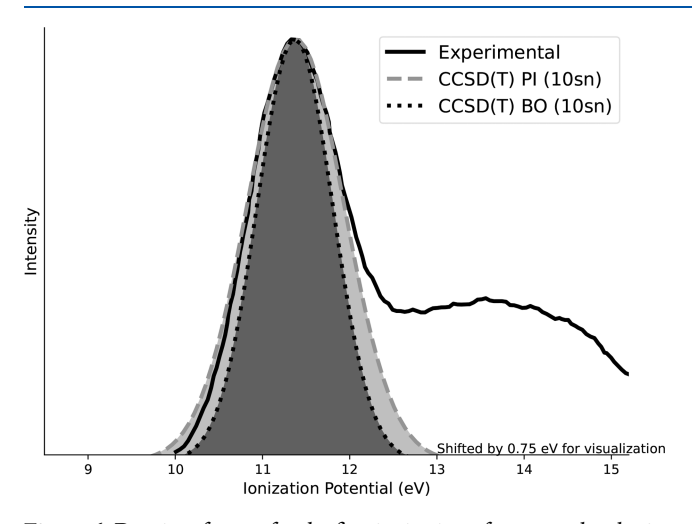


Figure 6. Density of states for the first ionization of water molecules in bulk liquid water. Values computed with CCSD(T) are compared against the experimental microjet photoelectron spectrum. ⁵ For clarity, we shift the CCSD(T) value by 0.7 eV (BO) and 0.75 eV (PI) for an easier theory-experiment comparison.

of the Supporting Information, we show that to properly converge the polarization contribution to the IP we would need to go beyond $3 \times 2 \times 1$ supercells of the current cell size (probably a $3 \times 3 \times 3$ for a total of 1728 molecules would be enough). Inspecting Table S4, an estimated error introduced by the finite size effects for the polarization contribution to the IP is over 0.5 eV. Another, less consequential approximation is the fact that we are not properly accounting for the nonadditive part

Table 1. Computed and Experimental IP of Bulk Liquid Water in eV, Including Correlation, Polarization, and Embedding Effects a

this work		literature	
PBE (BO)	10.61	$G_0W_0/\text{PBE (BO)}^8$	10.21
PBE (PI)	10.57	$G_0W_0/\text{PBE} (\text{PI})^8$	10.09
MP2 (BO)	10.80	$G_0W_0/\text{RSH (BO)}^8$	11.61
MP2 (PI)	10.76	$G_0W_0/\text{RSH (PI)}^8$	11.53
CCSD(T) (BO)	10.63	$PEqS/MP2-RI (BO)^{12,53}$	11.49
CCSD(T) (PI)	10.58	Exp 1 ⁵⁴	11.31
		Exp 2 ²	11.67
		Exp 3 ⁵	11.33

"PBE, MP2, and CCSD(T) (GTO basis set) are calculated with PySCF.

of the electronic dynamic correlation. In addition, the employment of approximate nonadditive kinetic energy functionals make our nonadditive energies somewhat approximate. Test calculations (see Supporting Information, Table S3) place this error at 0.1 eV. Dealing with all of these potential sources of error is beyond the scope of this study, and we believe that our IP results are accurate enough for our intended purposes.

To compare our results with the experimental photoelectron spectra, we simply report a histogram of the computed IPs, presented in Figure 6. We remark that the comparison between our calculated histograms and the experimental photoelectron spectrum is based on the assumption that the photoelectron cross section is independent of photon energy (Condon approximation). Additionally, we can identify the IP histograms with the joint density of states of neutral and cation states.

Inspecting Figure 6 and Table 1, we notice that the shape and broadening of the CCSD(T) density of states agrees well with the shape of the $1b_1$ peak of the experimental photoelectron spectrum of liquid water.⁵

The spectral shape can be further analyzed by reporting the full widths at half maxima (FWHM) for PBE, CCSD(T), and MP2, with the corresponding FWMH estimation from the spectral data available in the literature, ^{2,5,12,54} as shown in Table 2. The experimental fwhm's cover a range of 1.33–1.83 eV. All of

Table 2. Full Widths at Half Maxima (FWHM) in eV from the Computed Density of States and the Experimental Photoelectron Spectra

this work		literature	
PBE (BO)	1.04	PEqS/MP2-RI (BO) ^{12,53}	0.92
PBE (PI)	1.35	Exp 1 ⁵⁴	1.45
MP2 (BO)	1.04	Exp 2 ²	1.83
MP2 (PI)	1.30	Exp 3 ⁵	1.33
CCSD(T) (BO)	1.04		
CCSD(T) (PI)	1.31		

the calculations on the BO MD geometries delivered narrower FWHM's (on average 1.06 eV), while the PI MD geometries provide wider distributions with FWHM's in the range 1.31—1.35 eV, depending on the electronic structure method employed, a value much closer to the experimental result.

CONCLUSIONS

We calculated the IP of liquid water using an ab initio method based on subsystem DFT. Thanks to the subsystem DFT partitioning of the energy and electron density, we could dissect the IP into several meaningful contributions including meanfield Hartree—Fock, electronic correlation, embedding, and polarization of the environment.

Our method perfectly reproduces the broadening and overall spectral shape of the $1b_1$ peak of the photoelectron spectrum of water, clearly pointing to the inclusion of nuclear quantum effects as essential. Our predicted average IP improves upon the literature periodic $G_0W_0/{\rm PBE}$, but underestimates by few tens of eV the experimental value as well as the periodic $G_0W_0/{\rm RSH}$ and MP2 of cluster models.

We computed correlation coefficients between the IP contributions and intramolecular and intermolecular geometrical degrees of freedom that characterize the structure of the liquid. We found that the Hartree–Fock and electronic correlation contributions correlate more with intramolecular than with intermolecular degrees of freedom. The embedding and polarization contributions displayed stronger correlation with the intermolecular degrees of freedom, especially those of short-range character describing features of the first solvation shell.

Our simulations show for the first time that the IP of liquids such as water are composed of several contributions which have distinct physical origin. Our work finds relevance also beyond the basic understanding of ionized liquids. For example, it can be exploited to design geometrical descriptors to parametrize and predict ionization properties of liquids.

METHODS

The water structures considered in this work are taken from ref 8. They were obtained with ab initio molecular dynamics (AIMD) using either a path integral (PI) MD or a Born—

Oppenheimer (BO) MD. Note that the former includes nuclear quantum effects while in the latter all nuclei are treated as classical particles. Ten snapshots of the BO and PI MDs were selected for further analysis.

The embedding potentials for charged and neutral systems were obtained with embedded Quantum ESPRESSO (eQE)²⁶ employing ultrasoft pseudopotentials from the PSL pseudopotential library. ⁵⁸ We used the PBE functional ⁵⁹ for the evaluation of the additive and nonadditive exchange-correlation, and revAPBEK²³ for the nonadditive kinetic energy. Following previous benchmarking studies, 18,35 a total of 40 and 400 Ry were set as the energy cutoffs for the plane wave expansions of the molecular orbitals and the charge density, respectively. Embedding potentials represented on regular fast Fourier transform (FFT) grids (Cartesian grids) were further splined to the atom-centered Lebedev grids used by the molecular codes such as ADF⁶⁰ and PySCF.⁶¹ Therefore, the splined embedding potentials can be used in molecular-based codes for a selfconsistent field (SCF)⁶² ground state total energy calculation. Apart from eQE, SCF ground state calculations that utilize the aforementioned embedding potentials were carried out with ADF⁶⁰ and PySCF.⁶¹ To use the embedding potentials in molecular codes exploiting local atomic orbitals, matrix elements of the embedding potential over the atomic orbitals are computed as

$$v_{\rm emb}^{ij} = \langle \chi_i | v_{\rm emb} | \chi_j \rangle \tag{26}$$

where χ_i and χ_j denote general atom-centered basis functions. In the case of ADF these are Slater-type orbitals (STO) and in the case of PySCF Gaussian-type orbitals (GTO). For intrasubsystem exchange—correlation, the PBE⁵⁹ functional has been employed. We also use the following wave function-based methods: second order Møller—Plesset perturbation theory (MP2) and coupled-cluster singles and doubles with the perturbative inclusion of triples CCSD(T).⁶³ Calculations at the DFT, HF, MP2 and CCSD(T) level were performed in PySCF with the Gaussian-type orbital aug-cc-PVQZ basis-set. We also carried out DFT, HF, and MP2 calculations in ADF with the Slater-type orbital QZ4P basis set. In the main text, we feature the PySCF results, while the ADF results are reported in the Supporting Information.

We remark that when employing embedded wave function-based methods, such as CCSD(T) and MP2, the computation of the interaction energy with the environment is carried out with the corresponding wave function-derived electron density (i.e., we solve the so-called λ equations for CCSD).

The calculation of the polarization contribution to the IP was carried out using QEpy 64,65 through eqs 21 and 22. We used eDFTpy 66 to evaluate the nonadditive kinetic in eq 8 and exchange-correlation energies in eq 7 and the embedding potential in eq 19.

The nuclear quantum effects on the IP are calculated by computing the IP for the BO and PI snapshots with CCSD(T).

The correlation coefficients between the IP contributions and the molecular degrees of freedom were calculated using the NumPy library,⁶⁷ where the default Pearson correlation was used. The molecular degrees of freedom were evaluated with an in-house code based on pbcpy,⁶⁸ where the symmetric/antisymmetric vibration of water is the sum/difference of the OH bond lengths. The amount of donated and accepted H-bonds from the environment were determined in a way analogous to ref 18, with an oxygen—oxygen distance cutoff of

3.5 Å and an O-H distance cutoff of 1.5 Å between different molecules.

ASSOCIATED CONTENT

Data Availability Statement

The results for all calculations are available on Zenodo at the following DOI: https://zenodo.org/record/7994318.

Supporting Information

The Supporting Information is available free of charge at https://pubs.acs.org/doi/10.1021/acs.jpcb.2c07639.

Additional tables and figures; Effects of hole delocalization; Electronic (hole) couplings; Correlation coefficients between select contributions to the IP of liquid water and the distance to the n'th neighboring water molecule; Correlation coefficients between selected geometrical degrees of freedom and the electronic correlation contribution to the IP of liquid water; Vertical IP summarized for BO and PI snapshots; Estimate of the IP correction from nonadditive nonlocal xc and kinetic energy; Finite-size effects in the determination of the IP of liquid water (PDF)

AUTHOR INFORMATION

Corresponding Authors

Xuecheng Shao — Department of Chemistry, Rutgers University, Newark, New Jersey 07102, United States; oorcid.org/ 0000-0003-2215-0926; Email: xs161@newark.rutgers.edu

Johannes Neugebauer — Theoretische Organische Chemie, Organisch-Chemisches Institut and Center for Multiscale Theory and Computation (CMTC), Westfälische Wilhelms-Universität Münster, 48149 Münster, Germany; ◎ orcid.org/ 0000-0002-8923-4684; Email: j.neugebauer@unimuenster.de

Michele Pavanello — Department of Physics, Rutgers University, Newark, New Jersey 07102, United States; Department of Chemistry, Rutgers University, Newark, New Jersey 07102, United States; Orcid.org/0000-0001-8294-7481; Email: m.pavanello@rutgers.edu

Authors

Jessica A. Martinez B — Department of Chemistry, Rutgers University, Newark, New Jersey 07102, United States

Lukas Paetow — Theoretische Organische Chemie, Organisch-Chemisches Institut and Center for Multiscale Theory and Computation (CMTC), Westfälische Wilhelms-Universität Münster, 48149 Münster, Germany; Department of Chemistry, Rutgers University, Newark, New Jersey 07102, United States

Johannes Tölle — Division of Chemistry and Chemical Engineering, California Institute of Technology, Pasadena, California 91125, United States; orcid.org/0000-0002-2414-7758

Pablo Ramos — Department of Chemistry and Biochemistry, Queens College, City University of New York, Queens, New York 11367, United States; Department of Chemistry, Rutgers University, Newark, New Jersey 07102, United States

Complete contact information is available at: https://pubs.acs.org/10.1021/acs.jpcb.2c07639

Author Contributions

△J.A.M.B. and L.P. contributed equally to the work.

Note

The authors declare no competing financial interest.

ACKNOWLEDGMENTS

This work is supported by the U.S. Department of Energy, Office of Basic Energy Sciences, under Award Number DE-SC0018343 and the National Science Foundation grant number CHE-2154760. The authors acknowledge the Office of Advanced Research Computing (OARC) at Rutgers, The State University of New Jersey for providing access to the Amarel and Caliburn clusters and associated research computing resources that have contributed to the results reported here. URL: http://oarc.rutgers.edu. L.P. gratefully acknowledges PROMOS mobility funding. J.N. acknowledges funding through SFB 858 of the Deutsche Forschungsgemeinschaft (Project Z01). J.T. acknowledges funding by the Deutsche Forschungsgemeinschaft (DFG, German Research Foundation), 495279997.

REFERENCES

- (1) Ambrosio, F.; Miceli, G.; Pasquarello, A. Electronic levels of excess electrons in liquid water. *J. Phys. Chem. Lett.* **2017**, *8*, 2055–2059.
- (2) Perry, C. F.; Zhang, P.; Nunes, F. B.; Jordan, I.; von Conta, A.; Worner, H. J. Ionization Energy of Liquid Water Revisited. *J. Phys. Chem. Lett.* **2020**, *11*, 1789–1794.
- (3) Credidio, B.; Pugini, M.; Malerz, S.; Trinter, F.; Hergenhahn, U.; Wilkinson, I.; Thürmer, S.; Winter, B. Quantitative electronic structure and work-function changes of liquid water induced by solute. *Phys. Chem. Chem. Phys.* **2022**, *24*, 1310–1325.
- (4) Thurmer, S.; Shinno, T.; Suzuki, T. Valence Photoelectron Spectra of Liquid Methanol and Ethanol Measured Using He II Radiation. *J. Phys. Chem. A* **2021**, *125*, 2492–2503.
- (5) Thürmer, S.; Malerz, S.; Trinter, F.; Hergenhahn, U.; Lee, C.; Neumark, D. M.; Meijer, G.; Winter, B.; Wilkinson, I. Accurate vertical ionization energy and work function determinations of liquid water and aqueous solutions. *Chem. Sci.* **2021**, *12*, 10558–10582.
- (6) Öhrwall, G.; et al. The electronic structure of free water clusters probed by Auger electron spectroscopy. *J. Chem. Phys.* **2005**, *123*, 054310.
- (7) Guo, J.-H.; Luo, Y.; Augustsson, A.; Rubensson, J.-E.; Såthe, C.; Ågren, H.; Siegbahn, H.; Nordgren, J. X-Ray Emission Spectroscopy of Hydrogen Bonding and Electronic Structure of Liquid Water. *Phys. Rev. Lett.* **2002**, *89*, 137402.
- (8) Gaiduk, A. P.; Pham, T. A.; Govoni, M.; Paesani, F.; Galli, G. Electron affinity of liquid water. *Nat. Commun.* **2018**, *9*, 1–6.
- (9) Reddy, S. K.; Straight, S. C.; Bajaj, P.; Pham, C. H.; Riera, M.; Moberg, D. R.; Morales, M. A.; Knight, C.; Götz, A. W.; Paesani, F. On the accuracy of the MB-pol many-body potential for water: Interaction energies, vibrational frequencies, and classical thermodynamic and dynamical properties from clusters to liquid water and ice. *J. Chem. Phys.* **2016**, *145*, 194504.
- (10) Ziaei, V.; Bredow, T. Probing ionization potential, electron affinity and self-energy effect on the spectral shape and exciton binding energy of quantum liquid water with self-consistent many-body perturbation theory and the Bethe—Salpeter equation. *J. Phys.: Condens. Matter* **2018**, *30*, 215502.
- (11) Dal Corso, A. Pseudopotentials periodic table: From H to Pu. Comput. Mater. Sci. **2014**, *95*, 337–350.
- (12) Coons, M. P.; Herbert, J. M. Quantum chemistry in arbitrary dielectric environments: Theory and implementation of nonequilibrium Poisson boundary conditions and application to compute vertical ionization energies at the air/water interface. *J. Chem. Phys.* **2018**, *148*, 222834.
- (13) Bader, R. F. W. A quantum theory of molecular structure and its applications. *Chem. Rev.* **1991**, *91*, 893–928.
- (14) Silvestrelli, P. L.; Parrinello, M. Water Molecule Dipole in the Gas and in the Liquid Phase. *Phys. Rev. Lett.* **1999**, *82*, 3308–3311.

- (15) Elles, C. G.; Rivera, C. A.; Zhang, Y.; Pieniazek, P. A.; Bradforth, S. E. Electronic structure of liquid water from polarization-dependent two-photon absorption spectroscopy. *J. Chem. Phys.* **2009**, *130*, 084501.
- (16) Heller, J. M.; Hamm, R. N.; Birkhoff, R. D.; Painter, L. R. Collective oscillation in liquid water. *J. Chem. Phys.* **1974**, *60*, 3483–3486.
- (17) Garbuio, V.; Cascella, M.; Reining, L.; Del Sole, R.; Pulci, O. Ab initio calculation of optical spectra of liquids: many-body effects in the electronic excitations of water. *Phys. Rev. Lett.* **2006**, *97*, 137402.
- (18) P, S. K.; Genova, A.; Pavanello, M. Cooperation and Environment Characterize the Low-Lying Optical Spectrum of Liquid Water. *J. Phys. Chem. Lett.* **2017**, *8*, 5077–5083.
- (19) Nordlund, D.; Odelius, M.; Bluhm, H.; Ogasawara, H.; Pettersson, L.; Nilsson, A. Electronic structure effects in liquid water studied by photoelectron spectroscopy and density functional theory. *Chem. Phys. Lett.* **2008**, *460*, 86–92.
- (20) DiStasio, R. A.; Santra, B.; Li, Z.; Wu, X.; Car, R. The individual and collective effects of exact exchange and dispersion interactions on the ab initio structure of liquid water. *J. Chem. Phys.* **2014**, *141*, 084502.
- (21) Jacob, C. R.; Neugebauer, J. Subsystem density-functional theory. Wiley Interdiscip. Rev. Comput. Mol. Sci. 2014, 4, 325–362.
- (22) Tölle, J.; Severo Pereira Gomes, A.; Ramos, P.; Pavanello, M. Charged-cell periodic DFT simulations via an impurity model based on density embedding: Application to the ionization potential of liquid water. *Int. J. Quantum Chem.* **2019**, *119*, e25801.
- (23) Laricchia, S.; Fabiano, E.; Constantin, L.; Della Sala, F. Generalized gradient approximations of the noninteracting kinetic energy from the semiclassical atom theory: Rationalization of the accuracy of the frozen density embedding theory for nonbonded interactions. *J. Chem. Theory Comput.* **2011**, *7*, 2439–2451.
- (24) Wesolowski, T.; Warshel, A. Ab initio free energy perturbation calculations of solvation free energy using the frozen density functional approach. *J. Phys. Chem.* **1994**, *98*, 5183–5187.
- (25) Wesolowski, T. A.; Weber, J. Kohn-Sham equations with constrained electron density: an iterative evaluation of the ground-state electron density of interacting molecules. *Chem. Phys. Lett.* **1996**, 248, 71–76
- (26) Genova, A.; Ceresoli, D.; Krishtal, A.; Andreussi, O.; DiStasio, R. A., Jr.; Pavanello, M. eQE: An open-source density functional embedding theory code for the condensed phase. *Int. J. Quantum Chem.* **2017**, *117*, No. e25401.
- (27) Mi, W.; Shao, X.; Genova, A.; Ceresoli, D.; Pavanello, M. eQE 2.0: Subsystem DFT beyond GGA functionals. *Comput. Phys. Commun.* **2021**, 269, 108122.
- (28) Hutter, J.; Iannuzzi, M.; Schiffmann, F.; VandeVondele, J. cp2k: atomistic simulations of condensed matter systems. *Wiley Interdiscip. Rev. Comput. Mol. Sci.* **2014**, *4*, 15–25.
- (29) Iannuzzi, M.; Kirchner, B.; Hutter, J. Density Functional Embedding for Molecular Systems. *Chem. Phys. Lett.* **2006**, 421, 16–20.
- (30) Lundberg, M.; Siegbahn, P. E. M. Quantifying the effects of the self-interaction error in DFT: When do the delocalized states appear? *J. Chem. Phys.* **2005**, *122*, 224103.
- (31) Dinh, P. M.; Gao, C. Z.; Klüpfel, P.; Reinhard, P.-G.; Suraud, E.; Vincendon, M.; Wang, J.; Zhang, F. S. A density functional theory study of $Na(H_2O)_n$: an example of the impact of self-interaction corrections. *Eur. Phys. J. D* **2014**, *68*, 239.
- (32) Schmidt, T.; Kraisler, E.; Makmal, A.; Kronik, L.; Kümmel, S. A self-interaction-free local hybrid functional: Accurate binding energies vis-à-vis accurate ionization potentials from Kohn-Sham eigenvalues. *J. Chem. Phys.* **2014**, *140*, 18A510.
- (33) Cohen, A. J.; Mori-Sánchez, P.; Yang, W. Insights into current limitations of density functional theory. *Science* **2008**, *321*, 792–794.
- (34) Eschenbach, P.; Neugebauer, J. Subsystem density-functional theory: A reliable tool for spin-density based properties. *J. Chem. Phys.* **2022**, *157*, 130902.
- (35) Genova, A.; Ceresoli, D.; Pavanello, M. Avoiding fractional electrons in subsystem DFT based ab-initio molecular dynamics yields accurate models for liquid water and solvated OH radical. *J. Chem. Phys.* **2016**, *144*, 234105.

- (36) Solovyeva, A.; Pavanello, M.; Neugebauer, J. Describing long-range charge-separation processes with subsystem density-functional theory. *J. Chem. Phys.* **2014**, *140*, 164103.
- (37) Martyna, G. J.; Tuckerman, M. E. A reciprocal space based method for treating long range interactions in ab initio and force-field-based calculations in clusters. *J. Chem. Phys.* **1999**, *110*, 2810–2821.
- (38) Signorell, R.; Winter, B. Photoionization of the aqueous phase: clusters, droplets and liquid jets. *Phys. Chem. Chem. Phys.* **2022**, 24, 13438–13460.
- (39) Van de Walle, C. G.; Martin, R. M. Theoretical study of band offsets at semiconductor interfaces. *Phys. Rev. B* **1987**, 35, 8154–8165.
- (40) Makov, G.; Payne, M. C. Periodic boundary conditions in *ab initio* calculations. *Phys. Rev. B* **1995**, *51*, 4014–4022.
- (41) Miliordos, E.; Xantheas, S. S. An accurate and efficient computational protocol for obtaining the complete basis set limits of the binding energies of water clusters at the MP2 and CCSD(T) levels of theory: Application to (H $_2$ O) $_m$, m = 2–6, 8, 11, 16, and 17. J. Chem. Phys. **2015**, 142, 234303.
- (42) Howard, J. C.; Tschumper, G. S. Benchmark Structures and Harmonic Vibrational Frequencies Near the CCSD(T) Complete Basis Set Limit for Small Water Clusters: (H $_2$ O) $_{\rm n=2,\ 3,\ 4,\ 5,\ 6}$. J. Chem. Theory Comput. 2015, 11, 2126–2136.
- (43) Senthilkumar, K.; Grozema, F.; Bickelhaupt, F.; Siebbeles, L. Charge transport in columnar stacked triphenylenes: Effects of conformational fluctuations on charge transfer integrals and site energies. *J. Chem. Phys.* **2003**, *119*, 9809–9817.
- (44) Senthilkumar, K.; Grozema, F. C.; Guerra, C. F.; Bickelhaupt, F. M.; Lewis, F. D.; Berlin, Y. A.; Ratner, M. A.; Siebbeles, L. D. Absolute rates of hole transfer in DNA. *J. Am. Chem. Soc.* **2005**, *127*, 14894–14903.
- (45) Ambrosio, F.; Pasquarello, A. Reactivity and energy level of a localized hole in liquid water. *Phys. Chem. Chem. Phys.* **2018**, 20, 30281–30289.
- (46) Jackels, C. F. An ab initio potential?energy surface study of several states of the water cation. *J. Chem. Phys.* **1980**, 72, 4873–4884.
- (47) Li, C.; Paesani, F.; Voth, G. A. Static and Dynamic Correlations in Water: Comparison of Classical Ab Initio Molecular Dynamics at Elevated Temperature with Path Integral Simulations at Ambient Temperature. *J. Chem. Theory Comput.* **2022**, *18*, 2124–2131.
- (48) Blase, X.; Boulanger, P.; Bruneval, F.; Fernandez-Serra, M.; Duchemin, I. Erratum: "GW and Bethe-Salpeter study of small water clusters" [J. Chem. Phys. 144, 034109 (2016)]. J. Chem. Phys. 2016, 145, 169901.
- (49) Hermann, A.; Schmidt, W.; Schwerdtfeger, P. Resolving the optical spectrum of water: Coordination and electrostatic effects. *Phys. Rev. Lett.* **2008**, *100*, 207403.
- (50) Hahn, P.; Schmidt, W.; Seino, K.; Preuss, M.; Bechstedt, F.; Bernholc, J. Optical absorption of water: Coulomb effects versus hydrogen bonding. *Phys. Rev. Lett.* **2005**, *94*, 037404.
- (51) Ambrosio, F.; Guo, Z.; Pasquarello, A. Absolute Energy Levels of Liquid Water. *J. Phys. Chem. Lett.* **2018**, *9*, 3212–3216.
- (52) Chen, W.; Ambrosio, F.; Miceli, G.; Pasquarello, A. Ab initio Electronic Structure of Liquid Water. Phys. Rev. Lett. 2016, 117, 186401.
- (53) Paul, S. K.; Coons, M. P.; Herbert, J. M. Erratum: "Quantum chemistry in arbitrary dielectric environments: Theory and implementation of nonequilibrium Poisson boundary conditions and application to compute vertical ionization energies at the air/water interface" [J. Chem. Phys. 148, 222834 (2018)]. J. Chem. Phys. 2019, 151, 189901.
- (54) Kurahashi, N.; Karashima, S.; Tang, Y.; Horio, T.; Abulimiti, B.; Suzuki, Y.-I.; Ogi, Y.; Oura, M.; Suzuki, T. Photoelectron spectroscopy of aqueous solutions: Streaming potentials of NaX (X= Cl, Br, and I) solutions and electron binding energies of liquid water and X-. *J. Chem. Phys.* **2014**, *140*, 174506.
- (55) Paul, S. K.; Herbert, J. M. Probing Interfacial Effects on Ionization Energies: The Surprising Banality of Anion—Water Hydrogen Bonding at the Air/Water Interface. *J. Am. Chem. Soc.* **2021**, *143*, 10189—10202.

- (56) Ghosh, D.; Isayev, O.; Slipchenko, L. V.; Krylov, A. I. Effect of Solvation on the Vertical Ionization Energy of Thymine: From Microhydration to Bulk. *J. Phys. Chem. A* **2011**, *115*, 6028–6038.
- (57) Ghosh, D.; Roy, A.; Seidel, R.; Winter, B.; Bradforth, S.; Krylov, A. I. First-Principle Protocol for Calculating Ionization Energies and Redox Potentials of Solvated Molecules and Ions: Theory and Application to Aqueous Phenol and Phenolate. *J. Phys. Chem. B* **2012**, *116*, 7269–7280.
- (58) Dal Corso, A. Pseudopotentials periodic table: From H to Pu. Comput. Mater. Sci. 2014, 95, 337-350.
- (59) Perdew, J. P.; Burke, K.; Ernzerhof, M. Generalized Gradient Approximation Made Simple [Phys. Rev. Lett. 77, 3865 (1996)]. Errata:(1997) Phys. Rev. Lett. 1997, 78, 1396.
- (60) Te Velde, G. t.; Bickelhaupt, F. M.; Baerends, E. J.; Fonseca Guerra, C.; van Gisbergen, S. J.; Snijders, J. G.; Ziegler, T. Chemistry with ADF. *J. Comput. Chem.* **2001**, *22*, 931–967.
- (61) Sun, Q.; Berkelbach, T. C.; Blunt, N. S.; Booth, G. H.; Guo, S.; Li, Z.; Liu, J.; McClain, J. D.; Sayfutyarova, E. R.; Sharma, S.; et al. PySCF: the Python-based simulations of chemistry framework. *Wiley Interdiscip. Rev. Comput. Mol. Sci.* **2018**, *8*, e1340.
- (62) Purvis, G. D.; Öhrn, Y. The transition state, the electron propagator, and the equation of of motion method. *J. Chem. Phys.* **1976**, 65, 917–922.
- (63) Noga, J.; Bartlett, R. J. The full CCSDT model for molecular electronic structure. *J. Chem. Phys.* **1987**, *86*, 7041–7050.
- (64) Giannozzi, P.; et al. Advanced capabilities for materials modelling with QUANTUM ESPRESSO. *J. Phys.: Condens. Matter.* **2017**, 29, 465901.
- (65) Shao, X.; Andreussi, O.; Ceresoli, D.; Truscott, M.; Baczewski, A.; Campbell, Q.; Pavanello, M. QEpy: Quantum ESPRESSO in Python. 2023; https://gitlab.com/shaoxc/qepy, https://gitlab.com/shaoxc/qepy.
- (66) Shao, X.; Pavanello, M. 2023; https://gitlab.com/pavanello-research-group/eDFTpy, https://gitlab.com/pavanello-research-group/eDFTpy.
- (67) Harris, C. R.; et al. Array programming with NumPy. *Nature* **2020**, 585, 357–362.
- (68) Genova, A. PBCpy: a Python3 package providing some useful abstractions to deal with molecules and materials under periodic boundary conditions (PBC). 2018; https://pypi.org/project/pbcpy.

NOTE ADDED AFTER ASAP PUBLICATION

This paper originally published ASAP on June 2, 2023. The title was modified and a few corrections were made in the text, and a new version reposted on June 6, 2023.